

RESEARCH ARTICLE | JANUARY 03 2025

Reversing the acoustic contrast factor by tuning the medium can make focused beams trap cells in three dimensions

Shiyu Li ; Zhixiong Gong  



Physics of Fluids 37, 012003 (2025)

<https://doi.org/10.1063/5.0239229>



Articles You May Be Interested In

Rapid mixing in microchannel using standing bulk acoustic waves

Physics of Fluids (December 2019)

Towards 3D selective manipulation of cells and microparticles with spiraling holographic interdigitated transducers

J Acoust Soc Am (October 2021)

High-frequency single beam acoustical tweezers for 3D trapping and dynamic axial manipulation of cells and microparticles

J Acoust Soc Am (April 2021)



Physics of Fluids

Special Topics Open for Submissions

[Learn More](#)



Reversing the acoustic contrast factor by tuning the medium can make focused beams trap cells in three dimensions

Cite as: Phys. Fluids **37**, 012003 (2025); doi: [10.1063/5.0239229](https://doi.org/10.1063/5.0239229)
Submitted: 18 September 2024 · Accepted: 8 December 2024 ·
Published Online: 3 January 2025




View Online



Export Citation



CrossMark

Shiyu Li¹  and Zhixiong Gong^{1,2,a)} 

AFFILIATIONS

¹State Key Laboratory of Ocean Engineering, School of Ocean and Civil Engineering, Shanghai Jiao Tong University, Shanghai 200240, China

²Key Laboratory of Marine Intelligent Equipment and System, Ministry of Education, Shanghai, China

^{a)}Author to whom correspondence should be addressed: zhixiong.gong@sjtu.edu.cn

ABSTRACT

Three-dimensional (3D) selective trapping of particles and cells shows several potential applications such as reproductive cell selection, cell mechanics measurement, and *in vivo* rheology probes. Single-focused beams are a good candidate because of their simplicity, excellent selectivity, and strong trap. However, typical human cells in the water medium have the positive acoustic contrast factor and cannot be trapped in the focus of maximum intensity in a spherical focused beam as demonstrated recently [Gong and Baudoin, “Single beam acoustical tweezers based on focused beams: A numerical analysis of two-dimensional and three-dimensional trapping capabilities,” *Phys. Rev. Appl.* **18**, 044033 (2022)]. To achieve the 3D trapping and meanwhile keep the viability of cells, we propose to use a cell-friendly medium (i.e., iodixanol solution) to reverse the acoustic contrast factor to negative. Numerical experiments are conducted for the breast cancer cell (Michigan Cancer Foundation-7, MCF-7) with the computation of the three-dimensional (3D) acoustic radiation forces based on the angular spectrum method. It is shown that 3D trapping of MCF-7 in iodixanol medium with a single focused beam is possible, both in and beyond the Rayleigh regime. This work provides a solution to use a simple focused beam for 3D trapping of typical human cells, which may be beneficial to single-cell analysis, cellular phenotyping, precise assembly of different cells in tissue engineering, and controlled drug delivery.

Published under an exclusive license by AIP Publishing. <https://doi.org/10.1063/5.0239229>

I. INTRODUCTION

Selectively trapping of a single cell is fundamental to applications in the fields of biomedical and life science including determining the mechanical properties of living cells, reproductive cell selection, and *in vivo* rheology probes, to name but a few. However, this is quite challenging because typical cells are fragile and their sizes are down to a few tens of micrometers (e.g., the size of typical human cells is around 10 μm). The widely used technique to manipulate a single living cell called the micropipette aspiration¹ is developed separately by Vlès² and Mitchison and Swann,^{3–6} both with a focus on the measurement of mechanical properties of cell membranes. A recent perspective predicts that the micropipette aspiration technique will be performed for sequential single-cell measurements to help understand the effect of heterogeneity and anisotropy on deformability.⁷ Unfortunately, this technique suffers from three main challenges. First, the trapping force coming from the pressure gradient in and outside the micropipette sucks the cell with a mechanical deformation, which may break the membrane and kill the cells. Second, the physical contact between the

pipette and cells may cause cross-contamination and integration problems in a microscope. Third, the diameter of the micropipette should be different and specifically selected for typical cells of various sizes.

To overcome the issues of the contact-trapping of a single cell, several non-contact tweezing techniques are developed based on various fields, such as optic, acoustic, and magnetic fields. The optical tweezers technology^{8,9} has excellent selectivity and accuracy, but the use of high-intensity lasers inevitably causes photothermal damages^{10,11} and/or photochemical damages to cells.¹² This does not meet the criterion of living cells in the applications of the biomedical field. While magnetic tweezers are safe for biological samples, they generally require the use of magnetic compounds for pretag, which may change the biomechanical properties of the cell surface.¹³ Compared to optical and magnetical tweezers, acoustical tweezers have several advantages: (i) good biocompatibility. As is known that ultrasound is safe for human cells and tissues under a certain threshold, which can be demonstrated in the widely used ultrasonic medical imaging.¹⁴ A recent experiment shows the good viability of typical human cells after the

two-dimensional (2D) acoustic manipulation with a single beam.¹⁰ (ii) Free of pretag. Most of the materials are responsible for acoustic excitation. Hence, the acoustical tweezers can exert acoustic radiation force and/or acoustic streaming-induced dragged force on the cells for manipulation. (iii) Strong trap or large force. In general, the radiation pressure is the ratio of the field intensity over the speed. Since the sound velocity is five orders of magnitude smaller than that of light, the acoustic radiation force is several orders of magnitude larger than the optical radiation force at the same driving power.^{15,16} Hence, the acoustic field is a prior candidate for manipulating living cells.

Over the years, researchers have conducted extensive and in-depth research on acoustic tweezers based on standing waves.^{17–19} The experimental setup for standing wave tweezers requires two transducers or a transducer with a reflector to form a standing wave, and the target particles must be located between them.^{20–23} In addition, due to the existence of multiple equilibrium positions (i.e., pressure nodes or anti-nodes), multiple particles are usually trapped at the same time (i.e., collective manipulation), while the selective trapping is excluded.^{15,22,24} However, selective trapping is key to using acoustical tweezers to manipulate a single cell as implemented with the micropipette aspiration technique. Naturally, the focused beams are candidates for achieving selective trapping of particles in space akin to its optical counterpart.⁸ This is due to the physical properties of the focused beam with the acoustic energy localized into a small focal point, providing a large intensity gradient for particle trapping from all directions. The three-dimensional (3D) trapping with acoustical tweezers will be significant for precisely probing the cell biomechanics without the physical contact between the targeted cells and the micropipette or supporting slides. To this end, Gong and Baudoin reported the trapping properties of typical human cells in water with single focused-beam acoustical tweezers. However, it is not possible to trap a typical human cell in water in three dimensions, although the two-dimensional trapping in the lateral plane perpendicular to the beam axis is possible at special frequencies due to particle resonance.²⁵

The single focused-beam acoustic tweezers have the advantages of simplicity, excellent selectivity, and strong traps. It will be inspiring to extend the single focused beam for the 3D trapping of human cells since a recent report shows the broad applications and many setups of focused beams.²⁶ In addition, selective trapping of a single cell makes the foundation to precisely position cellular structures at the cell-sized level in 3D space for the study of cell–cell interactions and tissue engineering, like the atom-by-atom assembly with focused-beam optical tweezers.²⁷ Unfortunately, typical cells in water are repelled rather than trapped in focus in the focused field in three dimensions because the acoustic contrast factor Φ_{SW} is positive and cells will generally get trapped at the minimum amplitude of the pressure field.²⁵ It is a challenge for single focused-beam acoustic tweezers to achieve the trapping of typical human cells. It should be noteworthy that the criterion of the trapping ability on the acoustic contrast factor Φ_{SW} is only intuitive for the standing wave field in the Rayleigh regime since the pressure amplitude maximum agrees with the velocity minimum. Nevertheless, this is not true for a single-focused beam with the fields of pressure and velocities shown in Fig. 2 of Ref. 25. For example, the maximum amplitude of the pressure and total velocity fields both occur at the focus, which is different from the case for standing waves. Although the indication of the acoustic contrast factor will be limited for complex wave fields, it can still illustrate the trapping ability to a certain

extent, e.g., with a focused beam in the Rayleigh regime with the main contribution from the relative compressibility of cells to the surrounding medium. In this work, we demonstrate that by adding the iodixanol solution with proper concentration, the acoustic contrast factor of cells is reversed compared to that in the water medium. Hence, 3D trapping of typical human cells in the focus of a focused beam is possible and meanwhile with good viability. The results show that the 3D trapping of Michigan Cancer Foundation-7 (MCF-7) cells can be achieved by numerical experiments both in and beyond the Rayleigh regime.

The structure of this work is organized into four parts as follows: Sec. II briefly describes the calculation of the sound field based on the angular spectrum method (ASM) and recalls the analytical formula for three-dimensional acoustic radiation force. Section III A introduces the parameters of the focused beam transducer and the basic principle of cell trapping. Sections III B and III C state the trapping analysis of cells in and beyond the Rayleigh regime, respectively. The effect of the working frequency f_0 of the transducer on cell trapping was discussed in Sec. IV.

II. ACOUSTIC RADIATION FORCE BASED ON ANGULAR SPECTRUM METHOD

To trap the cells in three dimensions, we need to obtain restoring forces from all directions, which comes from the effect of the acoustic radiation force (ARF). The ARF F is the result of linear momentum change between the acoustic field and cells, which depends on the incident and scattered waves. Therefore, the starting point of the acoustic radiation force theory is to compute the acoustic scattering of target particles. There are several methods to calculate the scattering from a spherical particle in an arbitrary acoustic field, including the multipole expansion method (MEM)^{28–30} and the angular spectrum method (ASM).^{25,31,32} In the MEM, the incident wave is decomposed directly into spherical waves, while in the ASM, the incident wave is decomposed into a superposition of a series of plane waves with different directions. Although these two methods decompose the incident field in different ways, the equivalence between them has been demonstrated for the ARF.³³ In this paper, the ASM is used to calculate the three-dimensional ARF by using our homemade Matlab code²⁵ since it is efficient to calculate the acoustic field from a planar and finite-aperture transducer. The calculation of ARF can be summarized into four steps: (i) use the angular spectrum method (ASM) to decompose the incident wave into a series of plane waves. (ii) For each plane wave component, calculate the scattering field using prior knowledge of the scatterer. (iii) Simplify the incident and scattered waves using the far-field conditions, superimpose them to obtain the total sound field, and calculate the stress tensor based on these expressions. (iv) Calculate the integration of the stress tensor obtained in step (iii) on a closed sphere S_R , and ultimately obtain the expression of the ARF with three components in Cartesian coordinates $F_j, j = x, y, z$.

Here, we briefly review the angular spectrum method (ASM).^{25,31,32} For the ASM, it is mainly divided into three steps: (i) the fast Fourier transform (FFT). By the FFT, an arbitrary incident field on the source plane ($z = 0$) can be decomposed into the sum of plane waves with different directions. Therefore, we can get the angular spectrum at the source plane. Assuming that the incident sound pressure field is known at the source plane: $p_{in}|_{z=0} = p_{in}(x, y, 0)$, and the angular spectrum $S(k_x, k_y)$ of the source plane can be obtained by 2D Fourier transform

$$S(k_x, k_y) = \int_{-\infty}^{+\infty} \int_{-\infty}^{+\infty} p_{in}(x, y, 0) e^{-ik_x x - ik_y y} dx dy, \quad (1)$$

where k_x and k_y are the two components of the wave vector (\mathbf{k}). (ii) The propagation of angular spectrum. Since each angular spectral component $S(k_x, k_y)$ is a plane wave, the propagation of sound field between different angular spectral planes can be calculated by using the properties of plane waves as

$$S(k_x, k_y)|_{z=z_s} = S(k_x, k_y)|_{z=0} e^{ik_z z_s}, \quad (2)$$

where z_s represents the axial distance between the target plane (located at $z = z_s$) and the source plane (located at $z = 0$), and the k_z is the z component of the wave vector (\mathbf{k}). The wave vector components satisfy the relationship: $k_z = \sqrt{(k^2 - k_x^2 - k_y^2)}$ with the wavenumber k . The diagram of the procedure can refer to Fig. 6 in Ref. 32. (iii) The inverse fast Fourier transform (IFFT). The acoustic results are transformed from the wavenumber domain back to the frequency domain. According to the above three steps, we can calculate the sound field at any target position (x, y, z) as

$$p_{in}(x, y, z) = \frac{1}{4\pi^2} \iint_{k_x^2 + k_y^2 \leq k^2} S(k_x, k_y)|_{z=0} \times e^{ik_x x + ik_y y + i\sqrt{k^2 - k_x^2 - k_y^2} z} dk_x dk_y. \quad (3)$$

Here, the integration is within the range of $k_x^2 + k_y^2 \leq k^2$, which can eliminate the influence of evanescent waves. Considering the spherical geometry of the scatterer, it is necessary to select the spherical coordinate system (r, θ, φ) . Combining with Legendre's addition theorem,^{31,34} the incident field expression based on ASM can be described as

$$p_{in} = \frac{1}{\pi} \sum_{n=0}^{\infty} \sum_{m=-n}^n i^n H_{nm} j_n(kr) Y_n^m(\theta, \varphi). \quad (4)$$

Here, $j_n(kr)$ is the spherical Bessel function of the first kind, and the spherical harmonics $Y_n^m(\theta, \varphi)$ are expressed as the product of two basis functions

$$Y_{nm}(\theta, \varphi) = \sqrt{\frac{(2n+1)(n-m)!}{4\pi(n+m)!}} P_n^m(\cos\theta) e^{im\varphi}, \quad (5)$$

where $P_n^m(\cos\theta)$ is the associated Legendre function, and H_{nm} is the beam-shape coefficients determined by the incident wave

$$H_{nm} = \iint_{k_x^2 + k_y^2 \leq k^2} S(k_x, k_y) Y_n^{m*}(\theta_k, \varphi_k) dk_x dk_y, \quad (6)$$

where the $S(k_x, k_y)$ is the angular spectrum described above, and the asterisk stands for the complex conjugation.

Accordingly, the scattering field can be expressed as

$$p_{sc} = \frac{1}{\pi} \sum_{n=0}^{\infty} \sum_{m=-n}^n i^n H_{nm} A_n^m h_n^{(1)}(kr) Y_n^m(\theta, \varphi). \quad (7)$$

Here, A_n^m is the dimensionless partial wave coefficients. Finally, the total sound field $p_1 = p_{in} + p_{sc}$ can be expressed as

$$p_1 = \frac{1}{\pi} \sum_{n=0}^{\infty} i^n \left\{ j_n(kr) + A_n^m h_n^{(1)}(kr) \right\} \sum_{m=-n}^n H_{nm} Y_{nm}(\theta, \varphi). \quad (8)$$

Once the sound field is determined, the calculation of the ARF is possible. The general expression of the acoustic radiation force can be written as^{28,29,33}

$$\mathbf{F} = \iint_{S_R} \left\langle \left(\frac{\rho_0 \mathbf{v}_1^2}{2} - \frac{p_1^2}{2\rho_0 c_0^2} \right) \mathbf{n} - \rho_0 \mathbf{v}_1 (\mathbf{v}_1 \cdot \mathbf{n}) \right\rangle dS, \quad (9)$$

where S_R is any fixed surface that surrounds the scatterer, ρ_0 and c_0 are the density and sound speed of the surrounding medium, respectively, and \mathbf{n} is the outward unit normal vector. Note that the particle velocity \mathbf{v}_1 can be solved according to the following relation: $\mathbf{v}_1 = \nabla p / (i\rho\omega)$. By substituting Eq. (8) into Eq. (9), and combining the relationship between particle vibration velocity and sound pressure, the three-dimensional ARF expression of arbitrary acoustic field for a spherical particle can be obtained as follows:^{31,33}

$$F_x = \frac{1}{4\pi^2 \rho_0 k^2 c_0^2} \operatorname{Re} \left\{ \sum_{n=0}^{\infty} \sum_{m=-n}^n C_n \left(-b_{n+1}^{-m} H_{nm} H_{n+1, m-1}^* + b_{n+1}^m H_{nm} H_{n+1, m+1}^* \right) \right\}, \quad (10a)$$

$$F_y = \frac{1}{4\pi^2 \rho_0 k^2 c_0^2} \operatorname{Im} \left\{ \sum_{n=0}^{\infty} \sum_{m=-n}^n C_n b_{n+1}^m \left(H_{n, -m} H_{n+1, -m-1}^* + H_{nm} H_{n+1, m+1}^* \right) \right\}, \quad (10b)$$

$$F_z = -\frac{1}{2\pi^2 \rho_0 k^2 c_0^2} \operatorname{Re} \left\{ \sum_{n=0}^{\infty} \sum_{m=-n}^n C_n c_{n+1}^m H_{nm} H_{n+1, m}^* \right\}. \quad (10c)$$

Here, the coefficients are defined as

$$C_n = A_n + 2A_n A_{n+1}^* + A_{n+1}^*, \quad (11)$$

$$b_n^m = \sqrt{[(n+m)(n+m+1)] / [(2n-1)(2n+1)]}, \quad (12)$$

$$c_n^m = \sqrt{[(n+m)(n-m)] / [(2n-1)(2n+1)]}. \quad (13)$$

Because of the rotational symmetry for spherical particles, the partial wave coefficients here are $A_n^m = A_n$ (i.e., independent of m).^{29,32,33} In analogy with quantum mechanics, the scattering coefficients s_n are used for scattering problems with the relation $s_n = 1 + 2A_n$, $|s_n| = 1$ for a lossless scatterer.³⁵ For a typical human cell, the fluid sphere is a proper model²⁵ with the scattering coefficient as $s_n = -D_n^*/D_n$ ³⁶ and the explicit expression of D_n is

$$D_n = \rho_f k a j_n(ka/\gamma_c) h_n^{(1)'}(ka) - \rho(k a/\gamma_c) j_n'(ka/\gamma_c) h_n^{(1)}(ka), \quad (14)$$

where ρ_f is the density of the fluid sphere (i.e., cell), ka is the dimensionless frequency with a the radius, and $\gamma_c = c_f/c_0$ is the ratio of the sound velocity between the fluid sphere and the surrounding fluid.

It should be noted that the ARF formulas in Eq. (10) are general for arbitrary sizes of cells and arbitrary fields if the scattering coefficients and beam shape coefficients are known prior. For simplicity in

the field of acoustofluidics, the Rayleigh limit is often considered with the assumption that the dimensionless frequency $ka \ll 1$ (i.e., cell size much smaller than the wavelength). Hence, Eq. (10) can be simplified as

$$F_j \approx -\frac{\pi a^3}{3} \frac{\partial}{\partial j} \left(f_1 \frac{|p|^2}{\rho_0 c_0^2} - \frac{3}{2} f_2 \rho_0 |\mathbf{v}|^2 \right) - \frac{2\pi(ka)^6}{9\rho_0 c_0^2 k^3} \text{Im} \left[(f_1^2 + f_1 f_2) p \frac{\partial p^*}{\partial j} + \frac{3}{4} f_2^2 \rho_0 c_0^2 \left(v_x \frac{\partial v_x^*}{\partial j} + v_y \frac{\partial v_y^*}{\partial j} + v_z \frac{\partial v_z^*}{\partial j} \right) \right], \quad (15)$$

where $j = x, y,$ or z , and this expression is equivalent to Eq. (6) of Ref. 25. The second term $\sim (ka)^6$ (corresponding to the scattering force) is of much smaller order than the first term $\sim (ka)^3$ (corresponding to the gradient force). If only the first term dominates, Eq. (15) can be further reduced to the classical Gorkov theory³¹

$$\mathbf{F} = -\nabla U, \quad (16)$$

where U is the Gorkov potential defined as³⁷

$$U = \frac{4\pi a^3}{3} \left[f_1 \left(|p|^2 / 4\rho_0 c_0^2 \right) - f_2 (\rho_0 |\mathbf{v}|^2 / 4) \right]. \quad (17)$$

Here, $f_1 = (1 - \kappa_p / \kappa_0)$ and $f_2 = 3(\rho_p - \rho_0) / (2\rho_p + \rho_0)$ are the monopolar and dipolar coefficients, and κ_p and ρ_p are, respectively, the compressibility and density of microparticles. Note that Gorkov's theory can be considered as a special case for the general ARF formulas in Eq. (10), only considering the monopole and dipole terms of the gradient force.

III. TRAPPING OF TYPICAL HUMAN CELLS WITH FOCUSED BEAMS

A. Design of the focused-beam transducer

To selectively trap a cell in three dimensions, the acoustic field should localize its energy into a small region and have a large gradient for all directions. The spherical focused beam is a good candidate as introduced in Ref. 25. However, synthesizing an ideal spherical focused sound wave is difficult because we need to place transducers on a closed spherical surface around the focus, which greatly limits the application of acoustic tweezers. Here, we adopt the previous method of using acoustic holography to design a single focused beam with a finite aperture.^{25,32} As illuminated in Fig. 1 of Ref. 25, by using the source plane at $z = h$ ($z = 0$ is the focus point) to truncate the spherical beams, two sets of isophase electrodes will be obtained with a π phase shift. The two sets of electrodes will excite local vibrations on the piezoelectric substrate and produce the spherical focused beam based on Fresnel's principle. The shapes of two sets of electrodes with opposite phases can be derived from the following geometric relationship:

$$R_1 = \frac{1}{k} \sqrt{(C + 2n\pi)^2 - (kh)^2}, \quad (18)$$

$$R_2 = \frac{1}{k} \sqrt{[C + (2n + 1)\pi]^2 - (kh)^2}, \quad (19)$$

where C is the arbitrary constant, n is an integer, and the subscripts 1 and 2 represent the two sets of positive and negative electrodes. The

detailed analysis process can be referred to in the description of Gong and Baudoin.²⁵ Following a similar design, the transducer's frequency is $f_0 = 40$ MHz with the wavelength in water $\lambda = 37.5 \mu\text{m}$, which is proper for typical human cells with a radius of about $10 \mu\text{m}$. The advantage of using acoustic holography to synthesize a focused beam is that the designed transducer is a planar sound source, which is convenient for microfabrication and integration with a microscope platform. Unlike the focused acoustic vortexes, the two sets of electrodes that generate focused waves are concentric circles with radii that do not vary along the azimuthal angle. It can be found that if the frequency f_0 and focal length h are given, the aperture radius R_A and the geometry of the transducer electrodes can be determined according to Eqs. (18) and (19). Here, we choose the total number of each set of electrodes $N = 26$ (with $n \in [0, 26]$) and the focal length is $h_0 = 1$ mm, so the aperture radius of the transducer is $R_A = 1.72$ mm (see Fig. 1). For the width of the electrode, half of the distance between two consecutive electrodes is chosen as used in Ref. 38. Note that the 3D restoring forces are necessary to selectively trap a typical human cell in three dimensions with the designed focused-beam acoustic tweezers. In the following, the ability of cell trapping with this device will be discussed numerically in two cases: in and beyond the Rayleigh regime.

B. Cell trapping in the Rayleigh regime

It should be noted that the trapping ability of acoustical tweezers depends on the cell size ratio to the wavelength. Although the size of typical human cells is about $10 \mu\text{m}$, for simplicity, we choose different cell sizes for a given frequency of 40 MHz with a fixed wavelength λ as described in Sec. III A. This is equal to the cases with the real sizes of cells in the field at a lower frequency. In other words, we can decrease

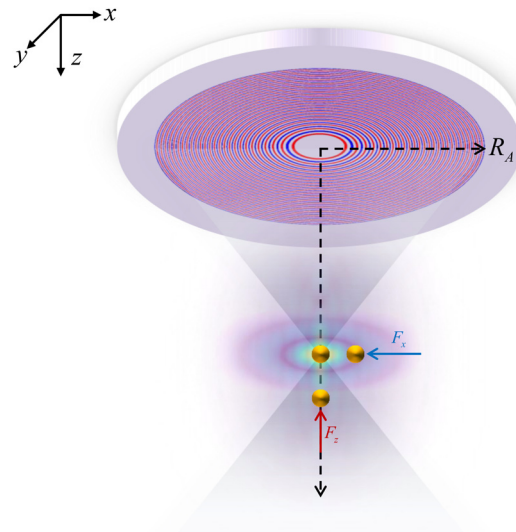


FIG. 1. Schematic of the 3D trapping with a focused beam. The two sets of electrodes in the red and blue colors on a piezo wafer are excited with the opposite phase (i.e., a π phase shift), and R_A is the aperture size of the transducer. The acoustic field is represented in a gradient color which shows that most energy is localized near the focal point. The red and blue arrows represent the restoring force in the respective axial and lateral directions, which ensures the 3D trapping of cells denoted by the small golden spheres.

the designed frequency of the transducer based on the required cell size ratio a/λ for the real cells. In the following, the terms of the cell or particle are used with the same acoustic properties.

For the 3D trapping in the Rayleigh regime, we calculate the Gorkov potential U and the corresponding gradient force using Eqs. (17) and (16), respectively. It should be noted that restoring forces from all directions will ensure stable trapping. Hence, the gradient force of a cell around the equilibrium position should have a negative derivative vs the spatial position, which corresponds to the minimum of the Gorkov potential.²⁵

As mentioned in Sec. II, when the radius of the cell is much smaller than the wavelength, the classical Gorkov theory can be used to calculate the acoustic radiation force,^{31,37} and the acoustic contrast factor Φ_{SW} in *standing waves* can be introduced for analysis.^{25,41}

$$\Phi_{SW} = \frac{5\rho_p - 2\rho_0}{2\rho_p + \rho_0} - \frac{\kappa_p}{\kappa_0}. \quad (20)$$

The sign of the acoustic contrast factor determines the direction of movement of the particles in a given acoustic gradient. Particles are trapped at pressure nodes (i.e., minimal pressure) when they have positive contrast factor $\Phi_{SW} > 0$. On the contrary, when particles have a negative acoustic contrast factor $\Phi_{SW} < 0$, they will be trapped at the pressure antinodes (i.e., maximum pressure). It should be noted that the acoustic contrast factor is only applicable in the Rayleigh regime.²⁵ For typical human cells in water, the acoustic contrast factor is positive. Therefore, cells will be pushed away from the focal point of a focused beam under the effect of the acoustic radiation force, making it impossible to achieve three-dimensional trapping under this situation.²⁵

In this section, we use the Gorkov theory to calculate the acoustic radiation force of breast cancer cells with radius $a = 0.001\lambda = 0.037 \mu\text{m}$ in both water and iodixanol medium. Recent studies have found that iodixanol solution is one kind of cell-friendly medium that could not only make the acoustic contrast factor reversed but also maintain the viability of cells in the solution.³⁹ The density (ρ_0 in the unit of kg/m^3) and the sound speed (c_0 in the unit of m/s) of the surrounding medium varies vs the concentration s of the iodixanol solution (s in the unit of percent) as

$$\rho_0 = 5.245s + 1005, \quad (21)$$

$$y = 2.557e^{-5}s^3 + 8.053e^{-3}s^2 - 0.7308s + 1507. \quad (22)$$

Based on Eq. (20), we have drawn the distribution diagram of the acoustic contrast factor Φ_{SW} of breast cancer cells in solutions with different densities and sound velocities, as shown in Fig. 2. The black curve described the corresponding density and sound velocity relationship of the iodixanol solution with different concentrations. It can be observed that the acoustic contrast factor Φ_{SW} is reversed to negative when the density is large enough (see the right-hand side), which corresponds to the situation of a higher concentration of the iodixanol solution). Consequently, the iodixanol solution of high concentration is a potential medium to make focused beams trap typical human cells in three dimensions in the Rayleigh regime.

Before we study the trapping ability of a focused beam in the iodixanol solution, the water medium is considered first as it is widely used in experiments. The acoustic pressure amplitude in the source plane is $p_0=1 \text{ MPa}$, and the designed frequency $f_0 = 40 \text{ MHz}$. Note that in the Rayleigh limit, the parameters are chosen with $a/\lambda = 0.001$

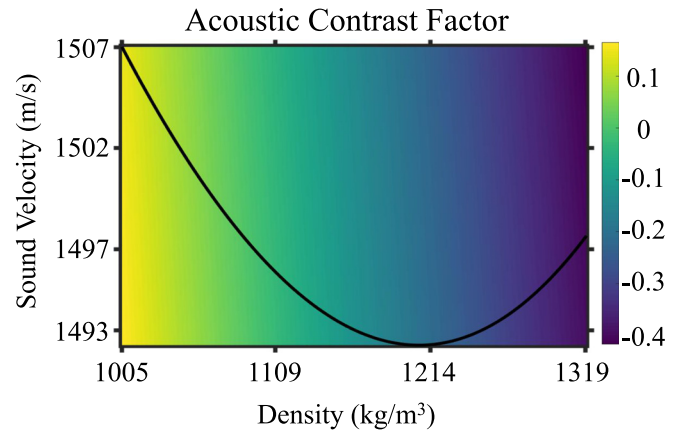


FIG. 2. Colormap of the acoustic contrast factors of breast cancer cells (MCF-7) in fluid mediums with different densities and sound velocities. The density and compressibility of breast cancer cells are $\rho_0 = 1068 \text{ kg/m}^3$ and $\kappa_0 = 400 \text{ TPa}^{-1}$. The black curve satisfies the properties of the iodixanol solution with various concentrations. The relationship between the acoustic parameters and the concentration of iodixanol can be found in Ref. 39.

for simplicity in the following numerical simulation to keep the same designed frequency at 40 MHz. This model is equivalent to a typical cell with a radius of $10 \mu\text{m}$ in a focused beam with a frequency of 0.15 MHz, leading to the same trapping ability in the present examples. The acoustic contrast factor of cells in water is $\Phi_{SW} = 0.18$, which is positive as shown in Table I. To recall the results of trapping cells in water with a focused beam, the Gorkov potential U in the propagation and lateral planes are given in the second and third columns of the upper row in Fig. 3. As observed, the Gorkov potential is maximum in the focus, which will push the cells out of the focus and cannot have the trapping ability. This is further validated by the axial and lateral acoustic radiation force vs spatial positions in the first and fourth columns of the upper row in Fig. 3. There are no restoring forces to keep the cells trapped at the focal point at $z = 0 \mu\text{m}$ or $x = 0 \mu\text{m}$. Hence, the focused beam cannot trap a typical human cell in water in the Rayleigh limit, which has been revealed in Ref. 25.

Next, we will discuss the trapping ability of breast cancer cells in a 60% iodixanol solution in the Rayleigh limit. The parameters are the same except for the surrounding medium from water to the 60% iodixanol solution. The density at this concentration is 1319.7 kg/m^3 and the sound speed is 1497.7 m/s , which makes the acoustic contrast factor reversed to negative with $\Phi_{SW} = -0.40$ as given in Table I. This provides an intuitive expectation of the possible trapping with a focused beam at the focus with the maximum pressure amplitude. This is demonstrated by computing the Gorkov potential and acoustic radiation forces as similar to the case of the water medium. As shown in the second and third columns of the lower row for the Gorkov potential in the propagation and lateral planes in Fig. 3, an obvious minimum value occurs at the focus for both cases, which will provide a trapping spot for the cell in the iodixanol solution. In addition, both the axial and lateral restoring forces are obtained to make the cell trapped stably at the focus. For a restoring force, taking the axial direction as an example, a negative force will pull the cell back if the cell is beyond the focus, while a positive force will push the cell if the cell is closer to the transducer plane (i.e., $z < 0$). Therefore, the focused

TABLE I. Acoustic parameters of breast cancer cells and mediums (water and 60% iodixanol) with the density ρ_0 , the longitudinal speed of sound c_l , and the compressibility $\kappa = 1/K$ with $K_f = \rho_p c_f^2$ for fluid material. The acoustic contrast factors Φ_{SW} are calculated with the middle values of the compressibility ($\kappa_0 = 400 \text{ TPa}^{-1}$) of the MCF-7 in Fig. 2.

| Material | ρ_0 (kg/m ³) | c_l (m/s) | κ (1/TPa) | Φ_{SW} |
|--|-------------------------------|---------------|------------------|-------------|
| Breast cancer cell (MCF-7) ⁴⁰ | 1068 | 1489.6–1569.7 | 380–422 | ... |
| Water | 1000 | 1489 | 451 | 0.18 |
| 60% iodixanol ³⁹ | 1319.7 | 1497.7 | 338 | −0.40 |

beam can trap typical human cells in a 60% iodixanol solution in three dimensions in the Rayleigh regime by reversing the acoustic contrast factor to negative with the trapping spot at the focus.

C. Cell trapping beyond the Rayleigh regime

The trapping ability beyond the Rayleigh limit is not as intuitive as the indicator of the Gorkov potential in the Rayleigh limit. In the Rayleigh limit ($ka \ll 1$), the gradient force [$\propto (ka)^3$] is dominant over the scattering force [$\propto (ka)^6$] as depicted in Eq. (15), while beyond the Rayleigh limit, the scattering force is comparable with the gradient force and depends on the acoustic scattering of cells. In this case, the general theory of acoustic radiation force in three dimensions given in Eqs. (10a)–(10c) is applied since the classical Gorkov theory is no longer applicable. The analysis of the trapping ability beyond the Rayleigh regime is more complicated, which will be discussed based on the schematic in Fig. 1. If the cell (marked by the golden ball) is located at a certain distance z_s downstream of the focal point ($z_s > 0$), a

negative axial acoustic radiation force F_z is required to pull the cell back to its equilibrium position (at or near the focal point) depicted by the red arrow. Similarly, if a cell deviates from its focal position in the lateral direction (i.e., $x_s > 0$), the corresponding negative restoring force F_x is necessary to pull the cell back to its lateral equilibrium position (see the blue arrow in Fig. 1). This provides a method to study the possible 3D trapping ability of cells in the following simulations. A summary of the calculation for the trapping ability beyond the Rayleigh regime can be divided into four steps: (i) preliminary validation of the axial trapping: Since the axial trapping is more difficult than lateral, we first verify the axial trapping vs different size ratios at a selected fixed position to see whether there is a negative axial radiation force F_z . The fixed position is a piece of prior information to check the possible restoring force. (ii) Preliminary validation of the lateral trapping: similar to the axial case but with the consideration in the lateral direction. (iii) Further confirmation of the axial trapping: take the cell with the selected radius corresponding to the negative radiation force in step (i), calculate the axial radiation force F_z vs z , and observe the

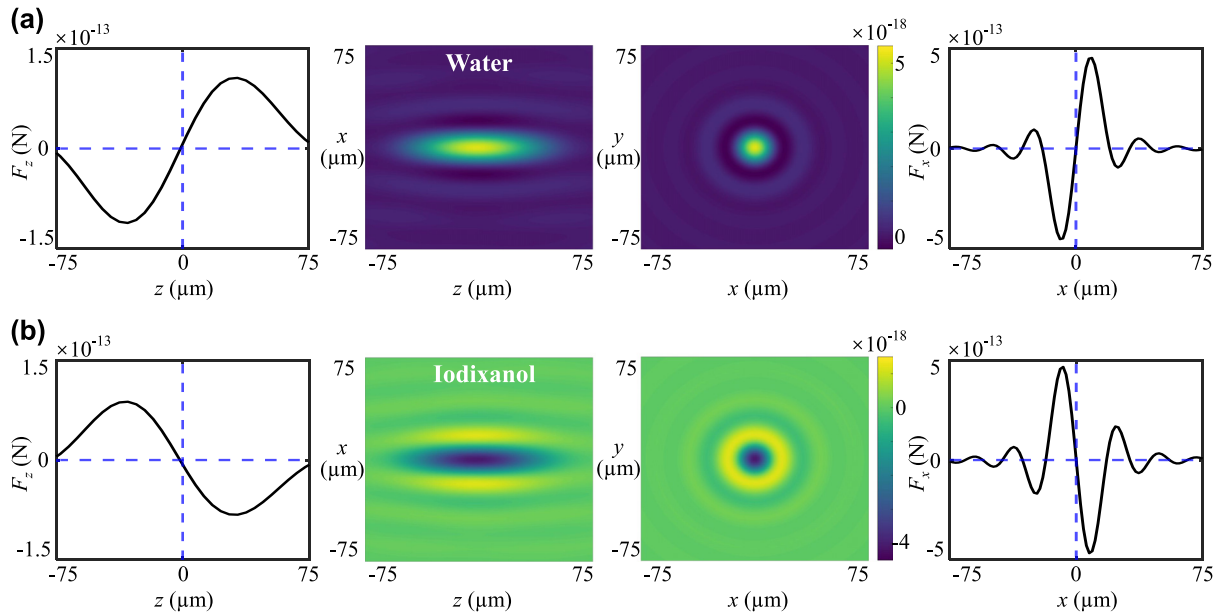


FIG. 3. The Gorkov potential U and the acoustic radiation force for a MCF-7 cell with a focused beam in the water and 60% iodixanol medium in the Rayleigh limit. The acoustic parameters are given in Table I. The ratio of the cell radius and the wavelength is 0.001. The upper row of (a) is the results of MCF-7 in water, while the lower row of (b) is the results in a 60% iodixanol solution. The curves in the first and fourth columns show the axial (F_z) and lateral (F_x) radiation forces vs spatial positions, respectively. The second and third columns represent the Gorkov potential in the x - z plane and x - y plane. The restoring forces in the axial and lateral directions occur for the iodixanol solution as shown in (b), providing the 3D trapping ability of MCF-7 cell with a focused beam.

04 January 2025 00:45:24

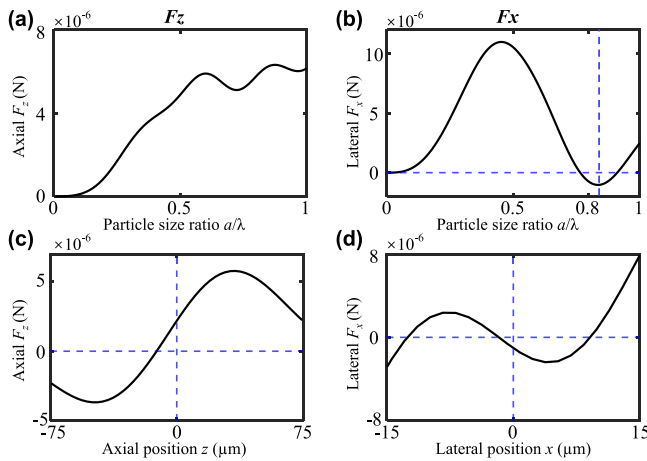


FIG. 4. The axial and lateral acoustic radiation forces of cells (MCF-7) in the water medium beyond the Rayleigh regime. The frequency of the sound field is $f_0=40$ MHz, and the sound pressure on the source plane is $p_0=1$ MPa. (a) The axial (F_z) and (b) lateral (F_x) acoustic radiation forces are calculated vs the cell size over the wavelength a/λ at a fixed position $(x_s, y_s, z_s) = (0, 0, 30)$ μm and $(x_s, y_s, z_s) = (8, 0, 0)$ μm in the respective axial and lateral directions. (c) The axial (F_z) and (d) lateral (F_x) acoustic radiation force vs the spatial position for a selected cell size $a/\lambda = 0.83$ as indicated by the vertical lines in (b). Only two-dimensional trapping of breast cancer cells is achieved with a single focused beam.

direction of the force around the focus to verify the trapping. (iv) Further confirmation of lateral trapping: Similar to step (iii), verify the lateral trapping. The above four steps [(i)–(iv)] correspond to the four subgraphs in Fig. 4 for the water medium and Fig. 5 for the iodixanol medium.

First, we study the trapping ability of the breast cancer cell (MCF-7) in the water medium. The frequency of the sound field is $f_0=40$ MHz, and the sound pressure on the source plane is $p_0=1$ MPa. The axial and lateral acoustic radiation forces of MCF-7 cells in water vs different cell size ratios a/λ with the range of $[0,1]$ are calculated as shown in (a) and (b) of Fig. 4. The axial and lateral radiation forces are computed at respective positions $(x_s, y_s, z_s) = (0, 0, 30)$ μm and $(x_s, y_s, z_s) = (8, 0, 0)$ μm . The results show that all the axial acoustic radiation forces are positive (i.e., $F_z > 0$), which means that the axial trapping of breast cancer cells in water cannot be achieved. As for the lateral acoustic radiation force F_x in Fig. 4(b), negative values around the ratio $a/\lambda = 0.83$ occur and the two-dimensional lateral trapping of MCF-7 cells may be possible in water. To further confirm the trapping ability, we compute the axial acoustic radiation force with z and lateral acoustic radiation force with x , respectively. The cell size ratio is selected as 0.83 indicated by the vertical dashed line in Fig. 4(b). The axial acoustic radiation force makes the cell in water move away from the focal point, while the lateral acoustic radiation force plays the role of a restoring force and allows the cell to move toward the neighbor of the focal point. Consequently, three-dimensional trapping of MCF-7 cells in water is not possible because there is no restoring force in the axial direction. The axial position could be fixed by using a membrane or glass slide in the experiment.¹⁰ Fortunately, the two-dimensional trapping of cells in water with a single focused beam is possible with selected size ratios, which agrees with the result in our previous work in Ref. 25.

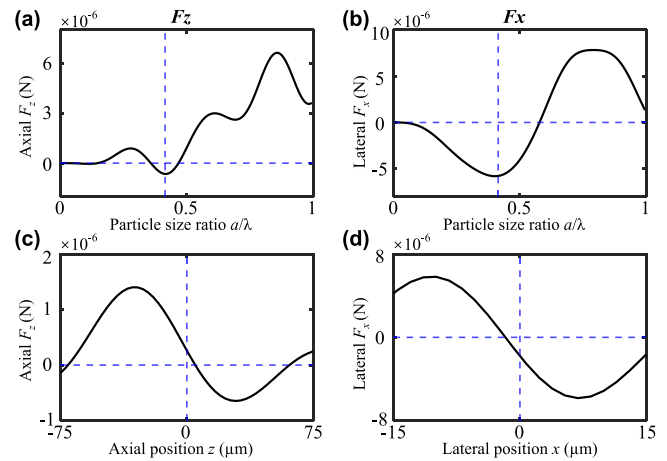


FIG. 5. The axial and lateral acoustic radiation forces of cells (MCF-7) in the 60% iodixanol medium beyond the Rayleigh regime. The frequency of the sound field is $f_0=40$ MHz, and the sound pressure on the source plane is $p_0=1$ MPa. (a) The axial (F_z) and (b) lateral (F_x) acoustic radiation forces are calculated vs the cell size over the wavelength a/λ at a fixed position $(x_s, y_s, z_s) = (0, 0, 30)$ μm and $(x_s, y_s, z_s) = (8, 0, 0)$ μm in the respective axial and lateral directions. (c) The axial (F_z) and (d) lateral (F_x) acoustic radiation force vs the spatial position for a selected cell size $a/\lambda = 0.41$ as indicated by the vertical lines in (a) and (b), respectively. The lateral radiation force is computed at the axial equilibrium position $z_s = 4.2$ μm in (d). Three-dimensional trapping of breast cancer cells is achieved with a single focused beam.

Since the 60% concentration of iodixanol solution makes the 3D trapping of cells in the Rayleigh regime with a single focused beam in Sec. III B, we further discuss the possibility of 3D trapping of cells in the same medium beyond the Rayleigh limit. Similar to the water medium, we first compute the 3D radiation forces on cells with different sizes in the iodixanol solution. As shown in Fig. 5(a), the axial acoustic radiation forces on MCF-7 cells in the iodixanol solution are negative at certain sizes. It means that the axial force can be taken as a restoring force to trap cells in this direction. This is completely different from the situation in water, where the axial acoustic radiation force is positive and the axial trapping cannot be achieved. When the cell radius is $a = 0.41\lambda = 15.35$ μm , the axial negative radiation force F_z exhibits the smallest value [see Fig. 5(a)], and at the same time, the lateral acoustic radiation force F_x is also negative as shown in Fig. 5(b). To further demonstrate the 3D trapping ability, the axial and lateral radiation forces vs the spatial positions at a selected size ratio $a/\lambda = 0.41$ are calculated in Figs. 5(c) and 5(d). Note that the lateral force is computed at the axial equilibrium position at $z_s = 4.2$ μm obtained in Fig. 5(c). It can be observed that negative gradients of both the axial and lateral radiation forces occur, which means the restoring forces will trap the cell around the focal point. Hence, by tuning the surrounding medium from water to the 60% iodixanol solution, a single focused beam can trap human cells with proper size ratios in three dimensions.

IV. AXIAL DISPLACEMENT BY FREQUENCY TUNING

Except for the 3D trapping, the axial displacement is important under the observation of a microscope in experiments since the imaging quality depends on the axial distance of the targets to the focal plane. However, precise physical motions are needed to improve the imaging quality. In this section, we propose a potential method to

change the axial position precisely by tuning the excitation frequencies without any physical motion of potential experimental setups. Based on the Fresnel principle and the design of the focused beam in Sec. III A, an approximation of the focal length depending on the excitation frequency $h(f)$ can be derived as follows (see details in Appendix):

$$h(f) = \alpha h_0 + \frac{C_1}{2k_0} \left(\alpha - \frac{1}{\alpha} \right), \quad (23)$$

where $\alpha = f/f_0$ is the ratio of the excitation frequency f to the designed frequency f_0 , k_0 and h_0 are the wavenumber and focal length at the designed frequency, and C_1 is a fixed constant for a given design of the transducer. If the excitation frequency is close to the design one, we have $\alpha \approx 1$, which leads to

$$h(f) \approx \left(h_0 + \frac{C_1}{k_0} \right) \alpha - \frac{C_1}{k_0}. \quad (24)$$

Therefore, the focal length $h(f)$ is changed linearly with the excitation frequency f , especially in the frequency range of [36,46] MHz. However, when the excitation frequency is out of the range, the $C_1/(2\alpha k_0)$ in the second term of Eq. (23) will change with α to some extent and make the analytical approximation indicated by the black solid line deviate from the red reference line in Fig. 6.

To further check the trapping ability with the excitation frequencies different from the designed one, we compute the acoustic field and radiation force in the iodixanol medium with a single focused beam as shown in Fig. 7. The acoustic pressure amplitudes in the propagation plan at three excitation frequencies are given in Figs. 7(a), 7(d), and 7(g), including the designed frequency $f_0 = 40$ MHz, below the designed frequency $f_- = 38$ MHz, and above the designed frequency $f_+ = 42$ MHz. When the excitation frequency is less than the designed frequency $f_- < f_0$, the focus position moves axially toward the source plane [see Fig. 7(a)]. While the excitation

frequency is higher than the designed frequency $f_+ > f_0$, the focus moves axially away from the source plane [see Fig. 7(b)]. In addition, the focal positions vs the excitation frequency from 30 to 50 MHz are calculated based on the angular spectrum method and are depicted by the blue dots in Fig. 6, which agree well with the analytical results in the frequency regime close to the design one $f_0 = 40$ MHz.

The axial acoustic radiation force vs the axial position z at the three selected frequencies are computed both in [panels (b), (e), and (h)] and beyond [panels (c), (f), and (i)] the Rayleigh regime. The radii of the cells are set as $a = 0.001\lambda = 0.037 \mu\text{m}$ in the Rayleigh regime and $a = 0.41\lambda = 15.35 \mu\text{m}$ beyond the Rayleigh regime. The designed focal positions and the axial trapped positions of cells are indicated by the green dashed lines and cyan dashed-dotted lines in the second and third rows of Fig. 7. As shown in Fig. 7, the cells in the iodixanol medium can be trapped in the axial direction in and beyond the Rayleigh limit. There is also lateral trapping at these axial equilibrium positions, which are not shown here for brevity. This demonstrates the possibility of trapping cells in an iodixanol medium with a single focused beam in three dimensions. It is noteworthy that the axial trapping positions of the cells at a selected excitation frequency in and beyond the Rayleigh limit are different because the scattering contribution to the radiation force is important for large sizes beyond the Rayleigh limit. In addition, the trapping positions are changed linearly in the Rayleigh limit as the trapping positions agree with the focal position (see the blue point in Fig. 6) and also beyond the Rayleigh limit (see the magenta squared points). Therefore, it is possible to keep the acoustic tweezers immovable and only change their excitation frequency to achieve axial displacement trapping of particles, which is crucial for the practical application of acoustic tweezers. By utilizing this feature, we do not need to change the physical position of the acoustic tweezers but only need to adjust their operating frequency f_0 to achieve dynamic control of particle trapping position.

V. CONCLUSIONS

In general, the single focused-beam acoustic tweezers cannot achieve the three-dimensional trapping of MCF-7 cells in the medium of water neither in nor beyond the Rayleigh regime. To benefit from the wide use of the focused beam and achieve the 3D trapping of cells, this work proposes to tune the surrounding medium into the iodixanol solution. The physical mechanism is to reverse the acoustic contrast factor of cells from positive in water to negative in iodixanol solution, which makes it possible to trap the cells at the maximum pressure amplitude in or near the focus of the focused beam. The 3D trapping of cells in the iodixanol solution is demonstrated by numerical simulations both in and beyond the Rayleigh regime, while only two-dimensional trapping can be achieved in the water medium for cells with certain sizes. There is no trapping for typical human cells in water with a focused beam in the Rayleigh limit as shown in Fig. 3. In addition, the axial trapping position can be tuned by changing the excitation frequency for a fixed design of the focused-beam acoustical tweezers. In a certain frequency regime including the designed one f_0 , the axial trapping position changes linearly vs the excitation frequency, which provides a potential method to move the trapped cells in the propagation direction without any physical motion of the experimental setups.

The present work provides a possible method to trap typical human cells in three dimensions while keeping the viability of the cells by using the iodixanol solution with a focused beam. It should be noted that a relatively high concentration of the iodixanol solution is

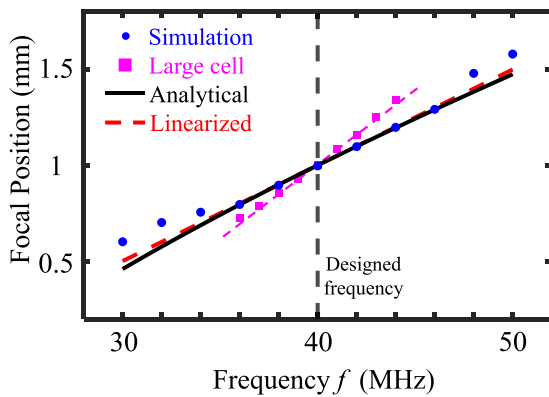


FIG. 6. Comparison of the focal length vs frequency f between the analytical calculations (black solid line) based on Eq. (23) (the black solid line) and numerical simulation based on the angular spectrum method (the blue dots). The red dashed line is given as a reference line to show the deviation of the analytical results from linearity when the excitation frequency is out of the frequency range [36,46] MHz. The trapping positions of particles in the Rayleigh limit agree with the focal position as indicated by the blue circle points. For particles beyond the Rayleigh limit, the trapping positions are given by the magenta squared points with a linear fitting with the magenta dashed line around the designed frequency.

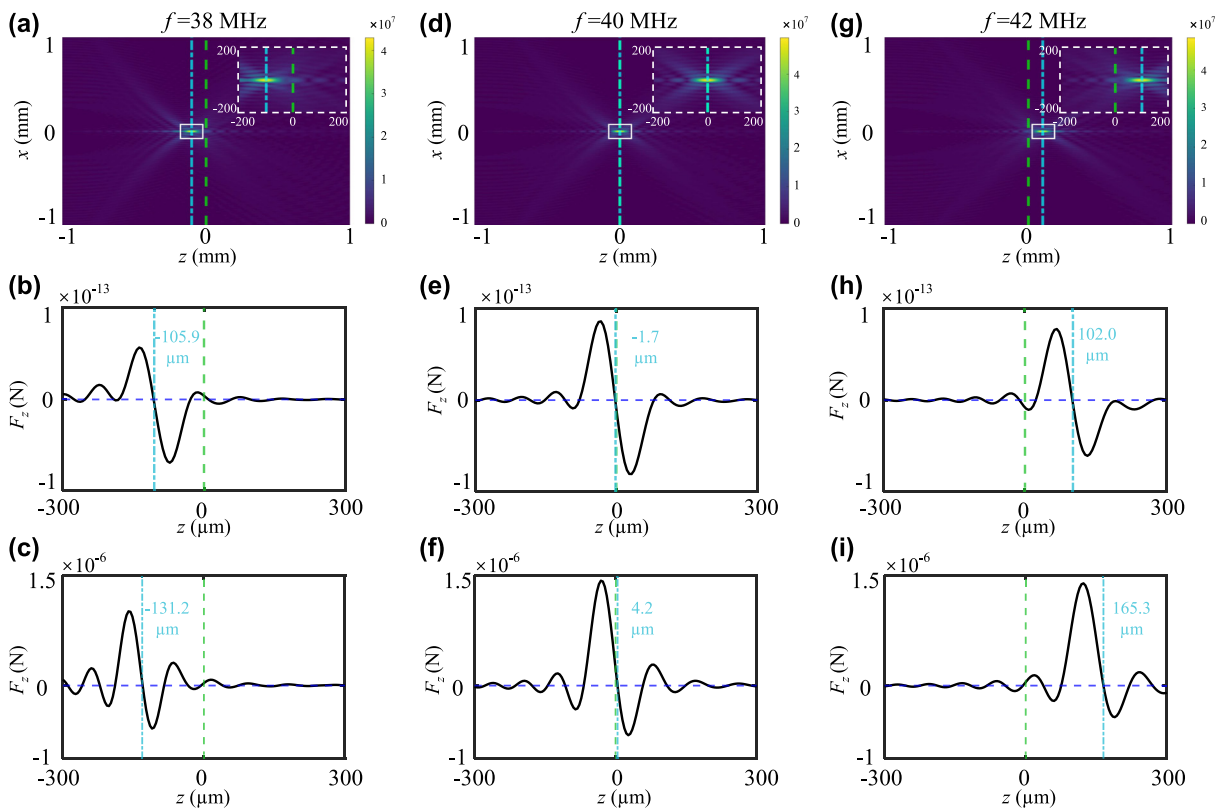


FIG. 7. (a), (d), and (g) The acoustic pressure amplitude distribution in (x, z) plane when the driving frequencies are $f = 38, 40,$ and 42 MHz, respectively. The insets in the upper right corner are partially enlarged views of the region near the focal point. The green dashed line marks the focus position of the designed frequency $f_0 = 40$ MHz, and the cyan dashed-dotted line represents the focus position corresponding to the three actual operating frequencies. The axial acoustic radiation force vs z at different driving frequencies in the Rayleigh regime [see (b), (e), and (h)] and beyond the Rayleigh regime [see (c), (f), and (i)]. In the simulations, the radii of breast cancer cells are selected as $a = 0.001\lambda = 0.037 \mu\text{m}$ in the Rayleigh regime and $a = 0.41\lambda = 15.35 \mu\text{m}$ beyond the Rayleigh regime. The axial equilibrium positions of the trapping cell are indicated by the cyan dashed-dotted lines. The lateral trapping is achieved and not presented here for brevity.

necessary to make the acoustic contrast factor of typical cells negative as shown in Fig. 2. A negative acoustic contrast factor will ensure the 3D trapping of cells in the iodixanol solution in the Rayleigh limit. However, for the case beyond the Rayleigh limit, the concentration of the iodixanol solution is expected to be larger than 50% to ensure the gradient force is dominant over the scattering force, leading to the 3D trapping with the present focused beam. In addition, for an acoustic field at such a high frequency, another nonlinear acoustic effect called acoustic streaming⁴² also plays an important role and is not helpful for particle or cell trapping. The streaming-induced Stokes drag force may reach the same order of magnitude as the acoustic radiation force and push the cells out of the trapped position ensured by the restoring radiation force. Fortunately, this can be achieved by optimizing the acoustic parameters such as pressure amplitude and excitation frequency, with the consideration of the combined effect of the acoustic radiation force and acoustic streaming.⁴³

ACKNOWLEDGMENTS

Z. Gong thanks for the support from the National Natural Science Foundation of China (No. 24Z990200542), Shanghai Jiao Tong University for the startup funding (Nos. WH220401017 and

WH22040121), and the XIAOMI Foundation. We thank Professor Per Augustsson from Lund University for the discussion of the acoustic parameters of the iodixanol solution.

AUTHOR DECLARATIONS

Conflict of Interest

The authors have no conflicts to disclose.

Author Contributions

Shiyu Li: Data curation (equal); Methodology (equal); Validation (equal); Writing – original draft (equal); Writing – review & editing (equal). **Zhixiong Gong:** Conceptualization (lead); Data curation (equal); Funding acquisition (lead); Investigation (equal); Methodology (equal); Project administration (lead); Resources (lead); Supervision (lead); Validation (equal); Writing – original draft (equal); Writing – review & editing (equal).

DATA AVAILABILITY

The data that support the findings of this study are available from the corresponding author upon reasonable request.

APPENDIX: DERIVATION OF THE RELATIONSHIP BETWEEN THE FOCAL LENGTH AND EXCITATION FREQUENCY

According to Eq. (19), we can obtain the formula for the maximum radius of the transducer R_A as

$$R_{\max} = \frac{1}{k} \sqrt{[kh + C_1]^2 - (kh)^2} = \frac{1}{k} \sqrt{2khC_1 + C_1^2}, \quad (\text{A1})$$

where $C_1 = (2 * 26 + 1)\pi = 53\pi$. We noticed that the following relationship holds for a fixed aperture size of a transducer with different excitation frequencies:

$$\frac{1}{k_0} \sqrt{2k_0 h_0 C_1 + C_1^2} = \frac{1}{k} \sqrt{2khC_1 + C_1^2}, \quad (\text{A2})$$

where $k_0 = 2\pi f_0 / c_0$ represents the wavenumber corresponding to the designed frequency f_0 , and $h_0 = 1$ mm is the design focal length. Then, the real focal length under the excitation frequency (which may be different from the designed one) can be written as

$$h = \frac{k}{k_0} h_0 + C_1 \left(\frac{k}{2k_0^2} - \frac{1}{2k} \right). \quad (\text{A3})$$

For convenience, the expression for the focal length h corresponding to arbitrary frequency f can be reorganized as

$$h(f) = \alpha h_0 + \frac{C_1}{2k_0} \left(\alpha - \frac{1}{\alpha} \right) \quad (\text{A4})$$

with $\alpha = k/k_0 = f/f_0$. When the frequency approaches the design frequency f_0 , we can use Taylor expansion to linearize Eq. (A4). Consider the following expansion

$$\begin{aligned} \frac{1}{\alpha} = \frac{f_0}{f} &= 1 / \left(1 + \frac{f - f_0}{f_0} \right) \\ &= 1 - \frac{f - f_0}{f_0} + O\left(\frac{f - f_0}{f_0}\right) \\ &= 2 - \alpha + O\left(\frac{f - f_0}{f_0}\right). \end{aligned} \quad (\text{A5})$$

By substituting Eq. (A5) into Eq. (A4) and retaining only the linear term, the linear relationship between focal length h and frequency ratio $\alpha = f/f_0$ can be obtained

$$h(f) \approx \left(h_0 + \frac{C_1}{k_0} \right) \alpha - \frac{C_1}{k_0}. \quad (\text{A6})$$

It should be noted that the above equation only holds near the design frequency f_0 .

REFERENCES

- R. M. Hochmuth, "Micropipette aspiration of living cells," *J. Biomech.* **33**, 15 (2000).
- F. Vlès, "Recherches sur une déformation mécanique des oeufs d'oursin," *Arch. Zool. Exp. Gin.* **75**, 421 (1933).
- J. Mitchison and M. Swann, "The mechanical properties of the cell surface: I. the cell elastimeter," *J. Exp. Biol.* **31**, 443 (1954).
- J. Mitchison and M. Swann, "The mechanical properties of the cell surface: II. The unfertilized sea-urchin egg," *J. Exp. Biol.* **31**, 461 (1954).
- J. Mitchison and M. Swann, "The mechanical properties of the cell surface: III. The sea-urchin egg from fertilization to cleavage," *J. Exp. Biol.* **32**, 734 (1955).
- J. Mitchison, "The mechanical properties of the cell surface: IV. The effect of chemical agents and of changes in pH on the unfertilized sea-urchin egg," *J. Exp. Biol.* **33**, 524 (1956).
- B. González-Bermúdez, G. V. Guinea, and G. R. Plaza, "Advances in micropipette aspiration: Applications in cell biomechanics, models, and extended studies," *Biophys. J.* **116**, 587 (2019).
- A. Ashkin, J. M. Dziedzic, J. E. Bjorkholm, and S. Chu, "Observation of a single-beam gradient force optical trap for dielectric particles," *Opt. Lett.* **11**, 288 (1986).
- A. Ashkin, "Acceleration and trapping of particles by radiation pressure," *Phys. Rev. Lett.* **24**, 156 (1970).
- M. Baudoin, J.-L. Thomas, R. A. Sahely, J.-C. Gerbedoen, Z. Gong, A. Sivery, O. B. Matar, N. Smagin, P. Favreau, and A. Vlandas, "Spatially selective manipulation of cells with single-beam acoustical tweezers," *Nat. Commun.* **11**, 4244 (2020).
- Y. Liu, D. Cheng, G. Sonck, M. Berns, C. Chapman, and B. Tromberg, "Evidence for localized cell heating induced by infrared optical tweezers," *Biophys. J.* **68**, 2137 (1995).
- A. Blázquez-Castro, "Optical tweezers: Phototoxicity and thermal stress in cells and biomolecules," *Micromachines* **10**, 507 (2019). <https://www.ncbi.nlm.nih.gov/pubmed/31370251>.
- D. Ahmed, C. Dillinger, A. Hong, and B. J. Nelson, "Artificial acousto-magnetic soft microswimmers," *Adv. Mater. Technol.* **2**, 1700050 (2017).
- M. Wiklund, "Acoustofluidics 12: Biocompatibility and cell viability in microfluidic acoustic resonators," *Lab Chip* **12**, 2018 (2012).
- M. Baudoin and J.-L. Thomas, "Acoustic tweezers for particle and fluid micro-manipulation," *Annu. Rev. Fluid Mech.* **52**, 205 (2020).
- D. Baresch, J.-L. Thomas, and R. Marchiano, "Observation of a single-beam gradient force acoustical trap for elastic particles: Acoustical tweezers," *Phys. Rev. Lett.* **116**, 024301 (2016).
- E. Trinh, "Compact acoustic levitation device for studies in fluid dynamics and material science in the laboratory and microgravity," *Rev. Sci. Instrum.* **56**, 2059 (1985).
- W. Xie, C. Cao, Y. Lü, and B. Wei, "Levitation of iridium and liquid mercury by ultrasound," *Phys. Rev. Lett.* **89**, 104304 (2002).
- S. Kabiri, A. Ghavidel, S. Derikvandi, F. Rezaei, A. Amjadi, and H. Hamzehpour, "Spontaneous rupture of polystyrene clusters trapped by acoustic tweezers: From experimental and simulation point of view," *Phys. Fluids* **36**, 033105 (2024).
- A. Hanson, E. Domich, and H. Adams, "Acoustical liquid drop holder," *Rev. Sci. Instrum.* **35**, 1031 (1964).
- H. Bruus, "Acoustofluidics 2: Perturbation theory and ultrasound resonance modes," *Lab Chip* **12**, 20 (2012).
- X. Ding, P. Li, S.-C. S. Lin, Z. S. Stratton, N. Nama, F. Guo, D. Slotcavage, X. Mao, J. Shi, F. Costanzo *et al.*, "Surface acoustic wave microfluidics," *Lab Chip* **13**, 3626 (2013).
- J. Wu, "Acoustical tweezers," *J. Acoust. Soc. Am.* **89**, 2140 (1991).
- A. Lenshof, M. Evander, T. Laurell, and J. Nilsson, "Acoustofluidics 5: Building microfluidic acoustic resonators," *Lab Chip* **12**, 684 (2012).
- Z. Gong and M. Baudoin, "Single beam acoustical tweezers based on focused beams: A numerical analysis of two-dimensional and three-dimensional trapping capabilities," *Phys. Rev. Appl.* **18**, 044033 (2022).
- Focused Ultrasound Foundation, "State of the field report" (2024), https://cdn.fusfoundation.org/2024/07/18084859/Focused-Ultrasound-Foundation-State-of-the-Field-Report-2024_July-17.pdf, accessed July 25, 2024.
- D. Barredo, V. Lienhard, S. De Leseleuc, T. Lahaye, and A. Browaeys, "Synthetic three-dimensional atomic structures assembled atom by atom," *Nature* **561**, 79 (2018).
- G. T. Silva, "An expression for the radiation force exerted by an acoustic beam with arbitrary wavefront (I)," *J. Acoust. Soc. Am.* **130**, 3541 (2011).
- D. Baresch, J.-L. Thomas, and R. Marchiano, "Three-dimensional acoustic radiation force on an arbitrarily located elastic sphere," *J. Acoust. Soc. Am.* **133**, 25 (2013).
- Z. Gong, P. L. Marston, and W. Li, "T-matrix evaluation of three-dimensional acoustic radiation forces on nonspherical objects in Bessel beams with arbitrary order and location," *Phys. Rev. E* **99**, 063004 (2019).

- ³¹O. A. Sapozhnikov and M. R. Bailey, "Radiation force of an arbitrary acoustic beam on an elastic sphere in a fluid," *J. Acoust. Soc. Am.* **133**, 661 (2013).
- ³²Z. Gong and M. Baudoin, "Three-dimensional trapping and dynamic axial manipulation with frequency-tuned spiraling acoustical tweezers: A theoretical study," *Phys. Rev. Appl.* **16**, 024034 (2021).
- ³³Z. Gong and M. Baudoin, "Equivalence between angular spectrum-based and multipole expansion-based formulas of the acoustic radiation force and torque," *J. Acoust. Soc. Am.* **149**, 3469 (2021).
- ³⁴G. Arfken and J. E. Romain, "Mathematical methods for physicists," *Phys. Today* **20**(5), 79 (1967).
- ³⁵P. L. Marston, "Scattering of a Bessel beam by a sphere," *J. Acoust. Soc. Am.* **121**, 753 (2007).
- ³⁶P. L. Marston, "Axial radiation force of a Bessel beam on a sphere and direction reversal of the force," *J. Acoust. Soc. Am.* **120**, 3518 (2006).
- ³⁷L. P. Gor'kov, "On the forces acting on a small particle in an acoustical field in an ideal fluid," *Sov. Phys. Dokl.* **6**, 773–775 (1962).
- ³⁸M. Baudoin, J.-C. Gerbedoen, A. Riaud, O. B. Matar, N. Smagin, and J.-L. Thomas, "Folding a focalized acoustical vortex on a flat holographic transducer: Miniaturized selective acoustical tweezers," *Sci. Adv.* **5**, eaav1967 (2019).
- ³⁹P. Augustsson, J. T. Karlsen, H.-W. Su, H. Bruus, and J. Voldman, "Iso-acoustic focusing of cells for size-insensitive acousto-mechanical phenotyping," *Nat. Commun.* **7**, 11556 (2016).
- ⁴⁰K. W. Cushing, F. Garofalo, C. Magnusson, L. Ekblad, H. Bruus, and T. Laurell, "Ultrasound characterization of microbead and cell suspensions by speed of sound measurements of neutrally buoyant samples," *Anal. Chem.* **89**, 8917 (2017).
- ⁴¹H. Bruus, "Acoustofluidics 7: The acoustic radiation force on small particles," *Lab Chip* **12**, 1014 (2012).
- ⁴²S. Li, W. Cui, T. Baasch, B. Wang, and Z. Gong, "Eckart streaming with nonlinear high-order harmonics: An example at gigahertz," *Phys. Rev. Fluids* **9**, 084201 (2024).
- ⁴³S. Li and Z. Gong, "Three-dimensional trapping of cells with focused-beam acoustical tweezers based on the combined effect of the acoustic radiation force and streaming-induced drag force," in *The 2024 Meeting of the Acoustical Society of China* (AIP, 2024).